RSC Advances

PAPER

View Article Online
View Journal | View Issue

Cite this: *RSC Adv.*, 2024, **14**, 5601

The antibacterial activity of three zeolitic-imidazolate frameworks and zinc oxide nanoparticles derived from them†

Pouya Khattami Kermanshahi and Kamran Akhbari *

Received 17th January 2024
Accepted 27th January 2024

DOI: 10.1039/d4ra00447g

rsc.li/rsc-advances

Zinc has been widely studied for its antibacterial properties due to its low toxicity, availability, and low cost. This research focused on analysing the antibacterial effects of three types of MOFs (metal–organic frameworks) with zinc as the central metal: ZIF-4, ZIF-7, and ZIF-8. The study found that ZIF-8 had the strongest antibacterial effect, while ZIF-7 had the weakest among them. These findings were consistent with the results of the ICP (inductively coupled plasma) analysis, which measured the amount of zinc released. Additionally, the antibacterial effect of ZIF-8 was found to be higher than that of zinc oxide species obtained from calcination of the compounds. Among the zinc oxide samples, ZnO nanoparticles which derived from ZIF-4 showed the highest antibacterial activity.

1. Introduction

Many different uses require biocidal materials (materials that can kill living organisms), such as creating packaging that can actively protect food, developing medical equipment, and producing membranes that resist biological buildup. Additionally, the growing problem of microorganisms becoming resistant to commonly used antibacterial medications is motivating researchers to create new types of antimicrobial agents.[1] There are two major challenges here; one is the ability of microorganisms to develop resistance to antimicrobial agents over time. This means that even when a new agent is developed, there is a risk that microorganisms will eventually become resistant to it as well. The second one is ensuring that the antimicrobial agent is effective against a wide range of microorganisms while being safe for human use and not harmful to the environment. Additionally the cost of the new agent is another limiting factor in the development of anti-microorganism substances.[2] Transition metals such as Cu, Zn, Ag, or Mn and also nanomaterials (like nanoparticles or metal–organic frameworks), which have a high surface area to volume ratio that includes these ions, have attracted increasing attention as infrequent bactericidal agents because effective conventional drugs have not kept pace with the progress of multidrug-resistant (MDR) bacteria.[3–5] As mentioned above, the design of materials that do not pose a risk to natural tissues while destroying bacteria is one of the important issues that need investigation. Unfortunately, most of the nanoparticles used so far fail due to the excessive release of metal ions, causing high toxicity in addition to their strong bactericidal effect. Therefore, it is necessary to find more effective and safer antibacterial agents to counter multidrug-resistant (MDR) microorganisms.[6] Hybrid composite materials obtained from organic and inorganic materials, like metal nanoparticles, have demonstrated bactericidal applications. Among them, most studies have focused on compounds derived from silver ions. Unfortunately, silver ions are toxic and pose dangers to human health and the environment. More recent studies have shifted towards the use of less hazardous metal ions, such as Zn^{2+}.[7] Although zinc ion causes cell toxicity in high concentrations, the presence of significant amounts of this ion (~4 g) in the human body creates the idea that this ion is far less toxic and is a suitable candidate for use in antibacterial applications.[8–10]

MOFs are an exciting area of research in chemistry, as they possess unique chemical and physical properties that can be adjusted by various parameters. Manipulating these parameters during their synthesis can result in MOFs with completely different characteristics. This has led many researchers to study MOFs due to their wide range of potential applications, such as catalysts,[11] electrochemical and chemical sensors,[12] encapsulating large molecules,[13] enzymes,[14,15] storing gas,[16,17] removal of hazardous heavy metals,[18] organic dyes and toxins,[19–21] water splitting,[22] exhibiting anti-bacterial and anti-cancer activities,[23–26] facilitating drug delivery[27–30] and *etc.* MOFs can be used as a source for releasing metal ions under controlled conditions. This controlled release helps maintain the cation concentration in the system at an optimum level—non-lethal for humans and safe for the environment.[31–33] It is important to note that MOFs, presumed to refer to precursor materials, serve as excellent precursors for the synthesis of nanometal oxide materials.[34,35]

School of Chemistry, College of Science, University of Tehran, P.O. Box 14155-6455, Tehran, Iran. E-mail: akhbari.k@ut.ac.ir; Fax: +98 21 66495291; Tel: +98 21 61113734

† Electronic supplementary information (ESI) available. See DOI: https://doi.org/10.1039/d4ra00447g

MOFs, when used as antibacterial agents, offer several benefits over typical disinfectants due to their extensive range of antibacterial properties, superior efficacy, sustained longevity, and their ability to regulate the release of metals.[6] In addition, it has been proven that MOFs are less toxic than other nanomaterials that act as antibacterials. Recently, the biological properties of MOFs (presumably referring to precursor materials) and the substances derived from them have gained attention.[36,37] Here, we report the antimicrobial activity of three Zn-based zeolitic-imidazolate frameworks (ZIF-4, ZIF-7, and ZIF-8), as well as ZnO samples obtained from their calcination. These three MOFs were selected due to their shared family origin, derived from nearly identical raw materials and methods, and extensively researched to date. Despite having distinct formulas and structures, exploring and comparing the antibacterial activity of these three MOFs present an intriguing aspect of the study. This article not only investigates the antibacterial property of the three ZIFs but also, in addition to this aspect, uses these materials for the preparation of nano ZnO, demonstrating effective antibacterial properties.

2. Materials and methods

2.1. Materials

All reagents consist of imidazole (98%), benzimidazole (98%), 2-methylimidazole (98%), $Zn(NO_3)_2 \cdot 6H_2O$ (98%), $Zn(CH_3COO)_2 \cdot 2H_2O$ (98%) and anhydrous *N*,*N*′-dimethylformamide (99.8%), ethanol (99,6%) for the synthesis were commercially available and were used as received.

2.2. Analysis

The Equinox 55 FT-IR spectrometer (Bruker, Bremen, Germany) was used to record IR spectra in ATR form, covering the range of 400–4000 cm^{-1} with 4.0 cm^{-1} resolution and 16 scan numbers. X-ray powder diffraction (PXRD) measurements were conducted using an X'pert diffractometer made by Philips, which utilized monochromatized Cu-Kα radiation ($\lambda = 1.54056$ Å) with a step size of 0.01671 (degree). The X-ray source was operated at a voltage and current of 40 kV and 30 mA, respectively, and Bragg–Brentano was used as source-detector geometry with a scintillation detector. Additional attachments such as an anti-scatter slit (1°), divergence slit (1°), monochromator, and Soller slit (0.04 rad) were also used. The samples were characterized using a scanning electron microscope (Philips XL 30) with gold coating. Simulated PXRD patterns based on single crystal data were prepared using the Mercury software. To investigate release of the Zn^{2+} of the samples, they were immersed in PBS solution in (0.0025 mg L^{-1}) for 2 days. The supernatant fluids of solutions were quantified based on the timing of 1, 4, 10, 24 and 48 hours. The Zn^{2+} ion concentrations of solutions were tested by ICP-MS. Antibacterial activity of samples was determined against both Gram-positive bacterial strains (*Staphylococcus aureus* or *S. aureus*) (ATCC 25923) and Gram-negative bacterial strains (*Escherichia coli* or *E. coli*) (ATCC 25922) using the agar well diffusion assay method. The microorganisms used for testing the antibacterial properties were grown in a nutrient broth at a temperature of 37 °C for 24 hours. Plates containing sterile Müller Hinton agar were prepared. Inoculum containing 10^8 CFU mL^{-1} of each bacterial culture was incubated on nutrient agar plates by a sterile swab. Afterward, sterilized stainless steel cork borers were used to create wells with a diameter of 4 mm in the agar medium. The compounds were then dissolved in a 5% DMSO solvent to achieve a concentration of 5000 μg mL^{-1}. Next, 50 μL of each sample was added to the wells, and the plates were incubated at a temperature of 37 °C for 24 hours. The effectiveness of the samples in inhibiting the growth of microorganisms was determined by comparing the size of the zone of inhibition.

2.3. Synthesis and activation of ZIF-4

The synthesis method mentioned in the previous literature was employed for synthesizing this compound.[38] 0.5 g of imidazole and 1.13 g of $Zn(NO_3)_2 \cdot 6H_2O$ were combined in a 150 mL autoclave, and 75 mL of DMF was added until completely dissolved and became clear. The autoclave was then placed in the oven. The oven temperature was raised to 130 °C at a rate of 5 °C per minute and held at this temperature for 48 hours, then decreased to room temperature at a rate of 0.1 °C per minute until a yellow precipitate formed. Subsequently, it was washed three times with 20 mL of DMF to remove excess ligands. For activation, the sample was placed in a vacuum oven at a temperature of 120 °C overnight. Yield: 0.70 g, 45% (based on the final product).

2.4. Synthesis and activation of ZIF-7

The synthesis method mentioned in the previous literature was employed for synthesizing this compound.[25] First, 0.946 g of benzimidazole in 20 mL of DMF and 0.878 g of $Zn(CH_3COO)_2 \cdot 2H_2O$ in 20 mL of distilled water were separately dissolved. Each solution underwent ultrasonic treatment for 5 minutes. The clear benzimidazole solution was then added dropwise to the clear $Zn(CH_3COO)_2 \cdot 2H_2O$ solution to obtain a white precipitate. For solvent exchange and activation, the resulting ZIF-7 powder was separated by centrifugation. It was then centrifuged twice with DMF, twice with distilled water (10 mL each time), and twice with ethanol (2.5 mL each time). Subsequently, it was placed in an oven at a temperature of 150 °C for 1 hour. The yield was 1.03 g, representing a 42% yield based on the final product.

2.5. Synthesis and activation of ZIF-8

The synthesis method mentioned in the previous literature was used for the synthesis of this compound.[39] In a standard solvothermal synthesis, a solution containing 0.656 g of $Zn(NO_3)_2 \cdot 6H_2O$ and 0.594 g of 2-methylimidazole in 50 mL of DMF was prepared. The resulting mixture was stirred until it formed a clear solution, and then transferred into a Teflon-lined autoclave with a capacity of 100 mL. The autoclave was then placed in the oven at a temperature of 140 °C for 24 hours. After synthesis, the product was centrifuged at 7000 rpm for 10 minutes and washed with 10 mL of ethanol (three times). The resulting pale yellow powder was activated in a vacuum oven for

12 hours at a temperature of 60 °C. The yield was 0.43 g, representing a 65% yield based on the final product.

2.6. Preparation of ZnO from ZIF materials

To obtain zinc oxide, 0.5 g of each synthesized ZIF sample was calcined in a porcelain crucible at 500 °C. The zinc oxide obtained from ZIF-4, ZIF-7, and ZIF-8 was 0.360 g, 0.298 g, and 0.334 g, respectively.

3. Results and discussion

Three Zn-based metal–organic frameworks, ZIF-4, ZIF-7, and ZIF-8, were synthesized solvothermally using three members of the imidazole family. Subsequently, activated samples were created to assess and compare the antibacterial characteristics of the products.

3.1. Material characterization

3.1.1. Powder X-ray diffraction (PXRD) analysis. ZIF-4, ZIF-7, and ZIF-8 were analyzed by PXRD to assess their crystallinity. The PXRD patterns of the three synthesized MOFs were found to be consistent with the simulated patterns, obtained using the Mercury software (Fig. 1). All three compounds used in this study are well-known and have been extensively discussed in previous studies regarding their structural features.[40–42] These observations serve as evidence for the accurate synthesis of the samples. In this study, ZIF-4 and ZIF-8, synthesized using the solvothermal method, exhibit a superior crystalline nature compared to ZIF-7, which was synthesized at room temperature. This conclusion is drawn from the information acquired through X-ray powder analysis. The peaks in the PXRD pattern of ZIF-7 are broader, suggesting the entry of particles into the nano phase. This observation is also clearly evident in scanning electron microscopy images, where ZIF-7 exhibits smaller dimensions compared to other samples (as discussed in the Crystal morphology section). The reason for modifying the synthesis procedure of ZIF-7, resulting in a less crystalline nature compared to the other two cases, is that when using the solvothermal method similar to the synthesis of ZIF-8, a gel product was obtained. This gel did not dry, preventing the possibility of conducting analyses. Additionally, three ZnO samples were characterized by PXRD (Fig. S1 in the ESI†). The XRD patterns, is in agreement with the typical wurtzite structure of ZnO (hexagonal phase, space group $P6_3mc$, JCPDS card no. 36-1451) with the lattice parameters (a = 3.24982(9) Å, c = 1.6021 Å, Z = 2).

3.1.2. Crystal morphology. Scanning electron microscope images were utilized to examine the morphology of the prepared samples (Fig. 2). ZIF-4 exhibits a spherical morphology with nano-sized grains growing on its surface (Fig. 2a). ZIF-7 is in the form of beads (Fig. 2b), and ZIF-8 presents nano-sized surfaces (Fig. 2c). The ZnO samples obtained from the calcination process of ZIF-4, ZIF-7, and ZIF-8 exhibit more uniform dimensions, and morphologically, they do not appear to resemble their parent materials (Fig. 3). It is evident that the ZnO sample obtained from ZIF-4 has uniform nanoparticle morphology with a narrow size distribution (Fig. 3a). However, ZnO samples obtained from ZIF-7 and ZIF-8 show some degree of nanoparticle agglomeration, and micro-sized particles were

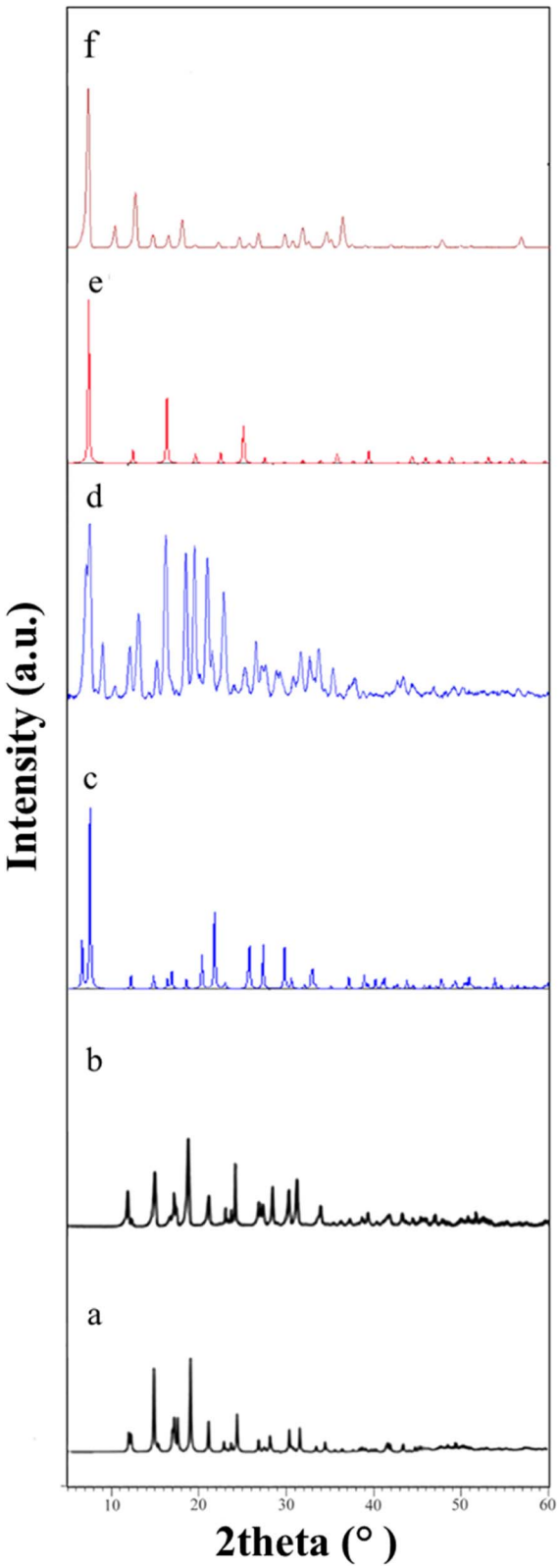

Fig. 1 PXRD patterns of (a) simulated of ZIF-4 (b) ZIF-4 (c) simulated of ZIF-7 (d) ZIF-7 (e) simulated of ZIF-8 (f) ZIF-8.

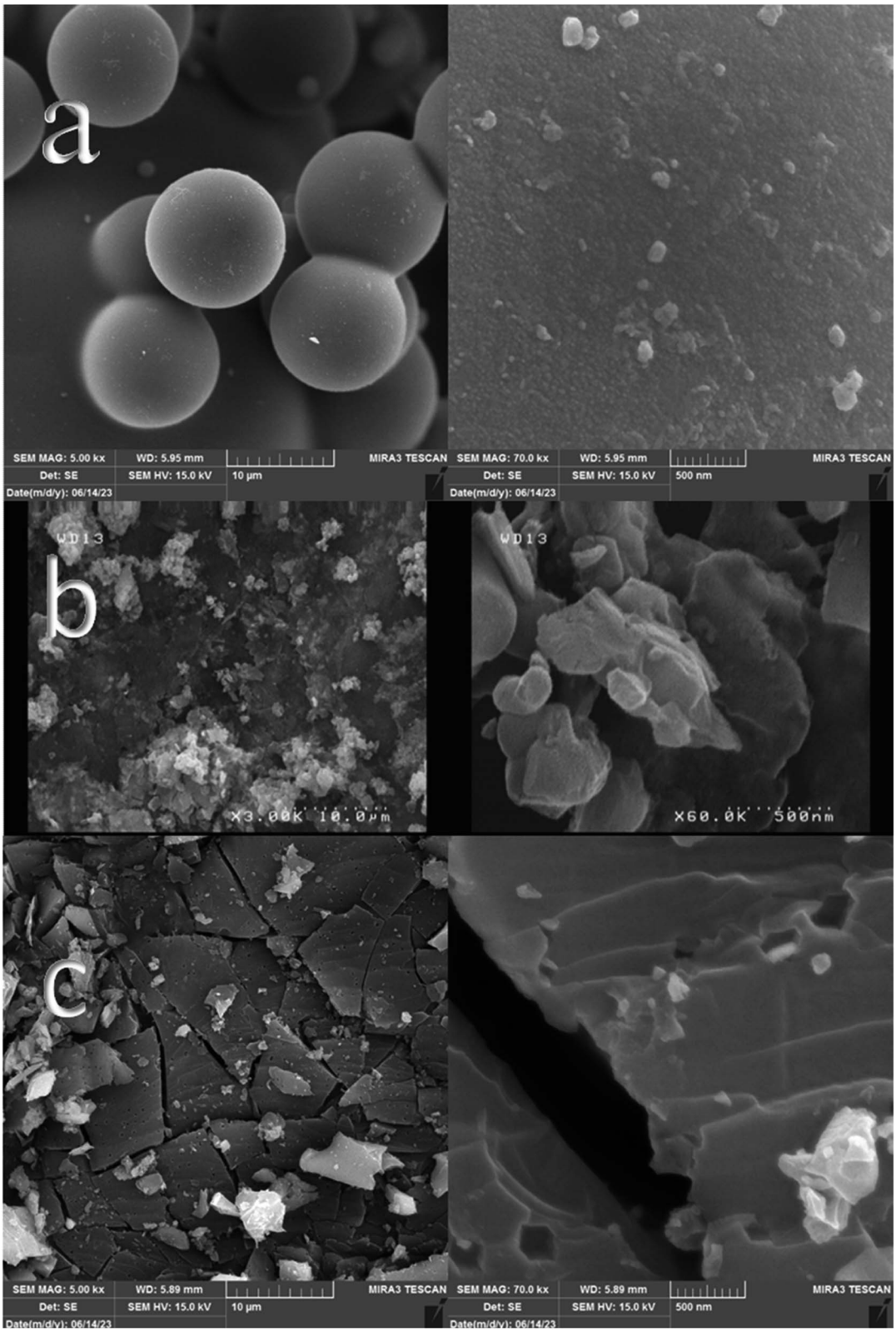

Fig. 2 SEM images of (a) ZIF-4 (b) ZIF-7 (c) ZIF-8.

formed in ZnO samples obtained from ZIF-7 and ZIF-8 (Fig. 3). The dispersion of ZIF-4 particles ranges from 555 to 6340 nm, with the highest frequency observed for particles in the range of 2000 to 2500 nm (Fig. S2 in the ESI†). For ZIF-7, particle dispersion is between 153 and 876 nm (Fig. S2 in the ESI†), exhibiting a more homogeneous distribution than the previous

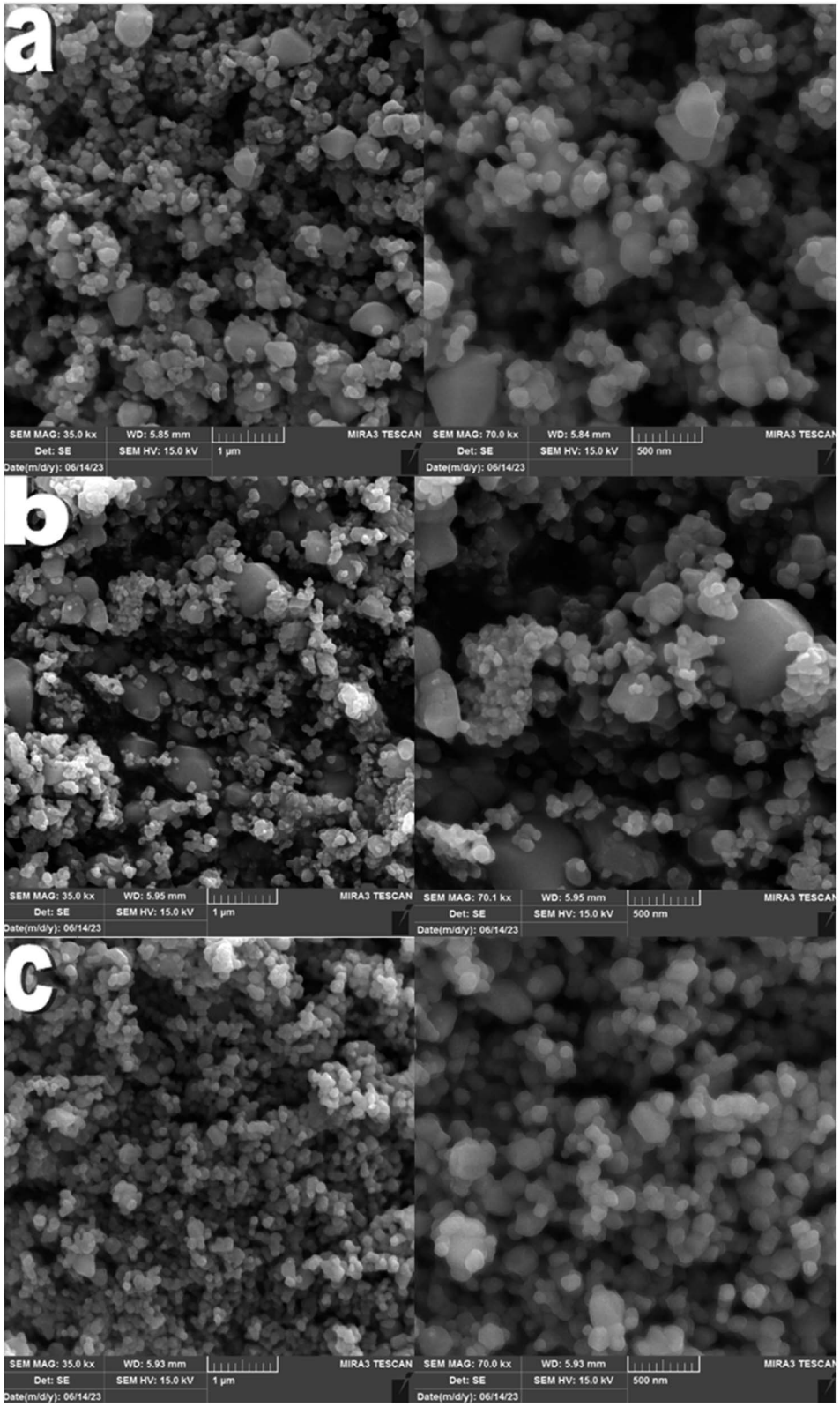

Fig. 3 SEM images of three types of zinc oxide derived from (a) ZIF-4, (b) ZIF-7 and (c) ZIF-8.

sample (ZIF-4). In this case, the highest dispersion is in the range of 400 to 450 nm. Regarding the ZIF-8 sample, particle dispersion ranges from 433 to 7014 nm, and the highest abundance is observed in the range of 1000 to 2000 nm (Fig. S2 in the ESI†). The dispersion of zinc oxide particles obtained from ZIF-4, ZIF-7, and ZIF-8 ranges from 45 to 441 nm, 39 to

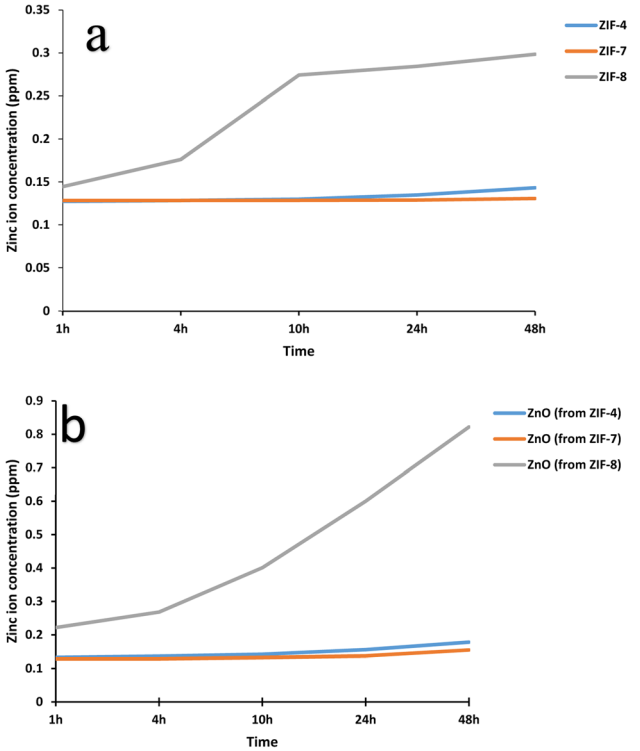

Fig. 4 The graph obtained from ICP analysis that shows the release of zinc ion in a period of 48 hours for (a) ZIF-4, ZIF-7 and ZIF-8 (b) ZnO samples drived from ZIF-4, ZIF-7 and ZIF-8.

760 nm, and 50 to 314 nm, respectively. This shows a higher uniformity compared to the synthesized ZIF samples (Fig. S3 in the ESI†).

3.1.3. Inductively coupled plasma (ICP) analysis. As expected, zinc ion release was higher in zinc oxide samples (Fig. 4). In both series, ZIF-8 and zinc oxide obtained from its calcination had the highest release. Fig. 4b shows the maximum release of Zn^{2+} from ZnO sample which was obtained from calcination of ZIF-8 after 48 hours to 1 ppm, while according to Fig. 4a, the maximum release for ZIF-8 after 48 hours is around 0.6 ppm. ZIF-4 and ZIF-7 samples did not show a significant Zn^{2+} release and their release level is reported to be constant for 48 hours, which shows that the structure of these two compounds is more stable. These studies have been a reconfirmation of the previous study of this research group on ZIF-7.[25] The release process of ZnO samples is similar to the ZIF samples derived from them, except for ZIF-4, where more Zn^{2+} release was observed. This observation could be attributed to its uniform nanoparticle morphology with a narrow size distribution, which is expected to have higher solubility and zinc ion release according to the Gibbs–Thompson relation.[43,44]

3.2. Antibacterial test

The agar well diffusion method was used to investigate the antimicrobial activity of ZIF-4, ZIF-7, ZIF-8, and their calcined samples. Their antibacterial properties were compared based on the zone of inhibition. The results of the antibacterial tests

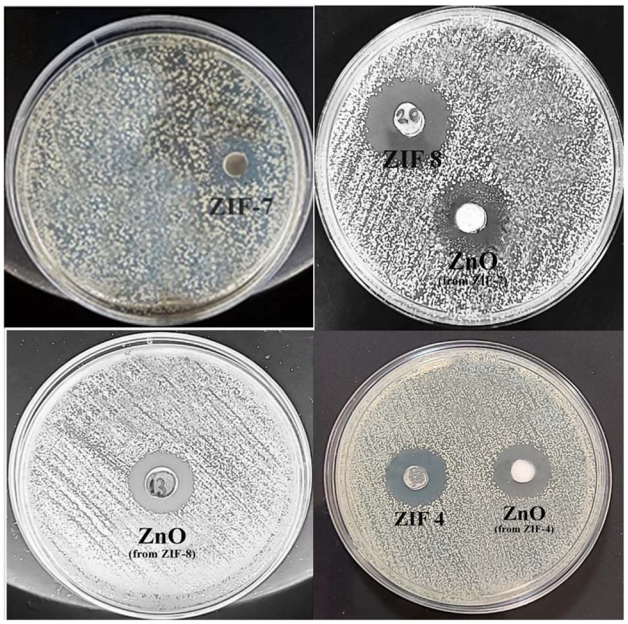

Fig. 5 The antibacterial test with the agar well diffusion assay method against *S. aureus* bacteria.

are presented in Fig. 5 and 6 and summarized in Table 1. These MOFs had a more pronounced effect on *S. aureus* as Gram-positive bacteria than on *E. coli* as Gram-negative bacteria. The results in Table 1 show that, except for ZIF-8, which also exhibited a weak effect on *E. coli* bacteria, the remaining samples only had an antibacterial effect on Gram-positive *S. aureus* bacteria. The challenge in transporting Zn^{2+} across the cell wall of Gram-negative bacteria arises from the presence of a lipopolysaccharide (LPS) outer membrane and a plasma inner membrane in the cell wall structure.[45,46] Thus, among the MOFs,

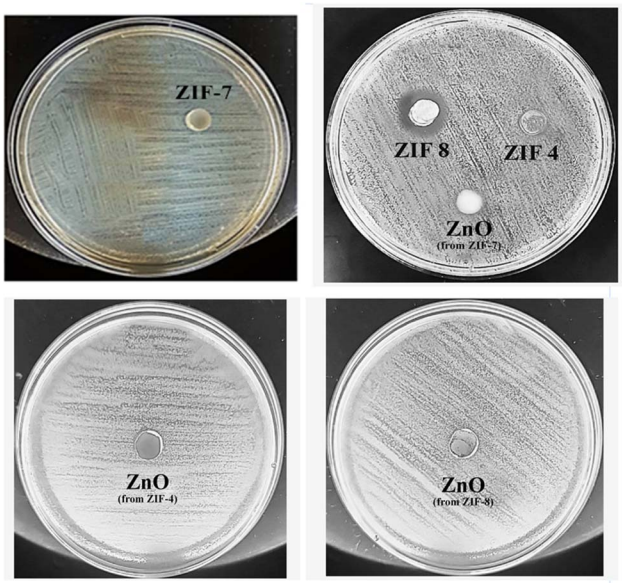

Fig. 6 The antibacterial test with the agar well diffusion assay method against *E. coli* bacteria.

Table 1 Summary of antibacterial test results (zone of inhibition) on two Gram-positive and Gram-negative bacteria and a comparison with previous reports

Sample	Concentration (mg mL^{-1})	*Staphylococcus aureus*	*Escherichia coli*	Ref.
Andrographis paniculate (leaves)	Not mentioned	6 mm	0 mm	47
Morinda citrifolia (leaves)	Not mentioned	7.3 mm	0 mm	47
Piper sarmentosum (leaves)	Not mentioned	9 mm	0 mm	47
Centella asiatica (leaves)	Not mentioned	5 mm	0 mm	47
Commercial ZnO NPs	20 000	13.1 mm	0 mm	48
$[Ni_2(pdc)_2(H_2O)_5]nH_2O\cdot DMF$	25 000	0 mm	11 mm	49
$[Ni_2(pdc)_2(H_2O)_5]nH_2O\cdot DMF$	50 000	14 mm	19 mm	49
$Cu(NO_3)_2\cdot 3H_2O$	10 000	28 mm	22 mm	50
Ag@ZIF-7	20 000	19 mm	12 mm	25
I_2@ZIF-7	20 000	17 mm	0 mm	25
I_2@MOF-808	50 000	19 mm	0 mm	24
Ag@ZnO	40 000	4 mm	8 mm	51
Ag@TiO_2	40 000	4 mm	8 mm	51
ZIF-4	20 000	16 mm	0 mm	This work
ZIF-7	20 000	15 mm	0 mm	This work
ZIF-8	20 000	20 mm	10 mm	This work
ZnO (from ZIF-4)	20 000	18 mm	0 mm	This work
ZnO (from ZIF-7)	20 000	15 mm	0 mm	This work
ZnO (from ZIF-8)	20 000	17 mm	0 mm	This work

ZIF-8 is ranked first with the highest bactericidal effect, and among the zinc oxide samples, the zinc oxide sample obtained from ZIF-8 shows a high release, resulting in a high bactericidal effect. This indicates that, in general, the structure of ZIF-8 is more unstable, and its zinc ion releases are higher than the other two ZIFs. After ZIF-8, ZIF-4 and ZIF-7 showed lower antibacterial properties. ZIF-4 and ZIF-8 had similar results in Zn^{2+} release and bactericidal assays. According to Table 1, the ZIF-8 sample had a similar effect on Gram-positive *S. aureus* bacteria as Ag@ZIF-7 in previous studies, and it was also a stronger antibacterial agent than I_2@ZIF-7, I_2@MOF-808 and $[Ni_2(pdc)_2(H_2O)_5]nH_2O\cdot DMF$, while this is a pure substance without doped agents and has an easier and cheaper synthesis.

The results of calcined samples are somewhat similar to the data observed for ZIF samples. However, it should be noted that, from the side-by-side examination of antibacterial studies and ICP analyses, it can be concluded that each sample showing more zinc ion release is a stronger antibacterial compound. The structural and morphological characteristics of ZIFs and ZnO samples also impact their antibacterial activity. Both the ZIF samples and the ZnO samples derived from them showed similar zinc ion release at 24 hours. Thus, as observed, each ZIF sample and the ZnO sample derived from it exhibited similar antibacterial activity. Except for the ZnO sample obtained from ZIF-4, the highest antibacterial activity was observed among the three ZnO samples. The highest antibacterial activity of this sample could be attributed to its uniform nanoparticle morphology with a narrow size distribution, resulting in more zinc ion release than the ZnO sample derived from ZIF-7.

4. Conclusion

Zinc ion is a chemical species whose antibacterial effect has been investigated for a long time. The low toxicity of this metal ion, along with its availability and cost-effectiveness, has made zinc compounds widely used for antibacterial purposes. In this study, three types of MOFs with zinc as the central metal, named ZIF-4, ZIF-7, and ZIF-8, was investigated as antibacterial agents. The results showed that ZIF-8 exhibited the highest antibacterial effect, and ZIF-7 was the weakest among them. These results are consistent with the zinc ion release data obtained from ICP analysis. Additionally, the antibacterial effect of ZIF-8 MOF was higher than that of the zinc oxide species obtained from the calcination of the ZIFs compounds. Among the ZnO samples derived from ZIFs compounds, although the ZnO sample derived from ZIF-8 showed the highest zinc ion release among the three ZnO samples and the ZnO sample derived from ZIF-4 exhibited the best antibacterial activity. The superiority of this sample should be attributed to its uniform nanoparticle morphology with a narrow size distribution, resulting in more zinc ion release than the ZnO sample derived from ZIF-7. It is also specified that despite having micrometer dimensions, ZIFs exhibit antibacterial characteristics similar to nano ZnO and, in fact, perform even better.

Conflicts of interest

There are no conflicts to declare.

Acknowledgements

The authors would like to acknowledge the financial support of University of Tehran for this research under grant number 01/1/389845. This work is based upon research funded by Iran National Science Foundation (INSF) under project No. 4024992.

References

1 S. Aguado, J. Quirós, J. Canivet, D. Farrusseng, K. Boltes and R. Rosal, *Chemosphere*, 2014, **113**, 188–192.
2 B. Waclaw, *Biophysics of Infection*, 2016, 49–67.
3 J. H. Jo, H.-C. Kim, S. Huh and Y. Kim, *Dalton Trans.*, 2019, **48**, 8084–8093.
4 C. Cattaneo, R. Di Blasi, C. Skert, A. Candoni, B. Martino, N. Di Renzo, M. Delia, S. Ballanti, F. Marchesi and V. Mancini, *Ann. Hematol.*, 2018, **97**, 1717–1726.
5 G. Ximing, G. Bin, W. Yuanlin and G. Shuanghong, *Mater. Sci. Eng., C*, 2017, **80**, 698–707.
6 Q. Zhao, L. Xin, Y. Liu, C. Liang, J. Li, Y. Jian, H. Li, Z. Shi, H. Liu and W. Cao, *J. Med. Chem.*, 2021, **64**, 10557–10580.
7 F. Akbarzadeh, M. Motaghi, N. P. S. Chauhan and G. Sargazi, *Heliyon*, 2020, **6**(1), e03231.
8 M. Hoop, C. F. Walde, R. Riccò, F. Mushtaq, A. Terzopoulou, X.-Z. Chen, A. J. deMello, C. J. Doonan, P. Falcaro and B. J. Nelson, *Appl. Mater. Today*, 2018, **11**, 13–21.
9 T. Kang, R. Guan, Y. Song, F. Lyu, X. Ye and H. Jiang, *LWT–Food Sci. Technol.*, 2015, **60**, 1143–1148.
10 C. Tamames-Tabar, D. Cunha, E. Imbuluzqueta, F. Ragon, C. Serre, M. J. Blanco-Prieto and P. Horcajada, *J. Mater. Chem. B*, 2014, **2**, 262–271.
11 V. Remya and M. Kurian, *Int. Nano Lett.*, 2019, **9**, 17–29.
12 P. G. Oorimi, A. Tarlani, R. Zadmard and J. Muzart, *Microchem. J.*, 2023, **189**, 108494.
13 Y. Yue, A. J. Binder, R. Song, Y. Cui, J. Chen, D. K. Hensley and S. Dai, *Dalton Trans.*, 2014, **43**, 17893–17898.
14 X. Zhang, R. Tu, Z. Lu, J. Peng, C. Hou and Z. Wang, *Coord. Chem. Rev.*, 2021, **443**, 214032.
15 Y. Noori and K. Akhbari, *RSC Adv.*, 2017, **7**, 1782–1808.
16 M. Parsaei, K. Akhbari and J. White, *Inorg. Chem.*, 2022, **61**, 3893–3902.
17 K. Akhbari and A. Morsali, *Mater. Lett.*, 2015, **141**, 315–318.
18 N. Abdollahi, G. Moussavi and S. Giannakis, *J. Environ. Chem. Eng.*, 2022, **10**, 107394.
19 H. Raza, I. Yildiz, F. Yasmeen, K. S. Munawar, M. Ashfaq, M. Abbas, M. Ahmed, H. A. Younus, S. Zhang and N. Ahmad, *J. Colloid Interface Sci.*, 2021, **602**, 43–54.
20 R. Ghasemzadeh and K. Akhbari, *Cryst. Growth Des.*, 2023, **23**(9), 6359–6368.
21 R. Ghasemzadeh and K. Akhbari, *New J. Chem.*, 2023, **47**, 15760–15770.
22 M. Ali, E. Pervaiz, T. Noor, O. Rabi, R. Zahra and M. Yang, *Int. J. Energy Res.*, 2021, **45**, 1190–1226.
23 S. Soltani and K. Akhbari, *JBIC, J. Biol. Inorg. Chem.*, 2021, 1–7.
24 M. Nakhaei, K. Akhbari and A. Davoodi, *CrystEngComm*, 2021, **23**, 8538–8545.
25 A. Davoodi, K. Akhbari and M. Alirezvani, *CrystEngComm*, 2023, **25**, 3931–3942.
26 R. W.-Y. Sun, M. Zhang, D. Li, M. Li and A. S.-T. Wong, *J. Inorg. Biochem.*, 2016, **163**, 1–7.
27 K. Kadota, J. Y. Tse, S. Fujita, N. Suzuki, H. Uchiyama, Y. Tozuka and S. Tanaka, *ACS Appl. Bio Mater.*, 2023, **6**(9), 3451–3462.
28 M. Parsaei and K. Akhbari, *Inorg. Chem.*, 2022, **61**, 14528–14543.
29 M. Parsaei and K. Akhbari, *Inorg. Chem.*, 2022, **61**, 5912–5925.
30 M. Parsaei and K. Akhbari, *Inorg. Chem.*, 2022, **61**, 19354–19368.
31 Y. Hara, M. E. Castell-Perez and R. G. Moreira, *J. Food Sci.*, 2023, **88**(6), 2512–2522.
32 M. Parsaei, K. Akhbari and J. White, *J. Mol. Struct.*, 2023, **1283**, 135224.
33 S. M. Mousavi, S. A. Hashemi, F. Fallahi Nezhad, M. Binazadeh, M. Dehdashtijahromi, N. Omidifar, Y. Ghahramani, C. W. Lai, W.-H. Chiang and A. Gholami, *Materials*, 2023, **16**, 4685.
34 E. Mirzadeh and K. Akhbari, *CrystEngComm*, 2016, **18**, 7410–7424.
35 M.-L. Hu, M. Y. Masoomi and A. Morsali, *Coord. Chem. Rev.*, 2019, **387**, 415–435.
36 K. Gwon, I. Han, S. Lee, Y. Kim and D. N. Lee, *ACS Appl. Mater. Interfaces*, 2020, **12**, 20234–20242.
37 H.-S. Wang, Y.-H. Wang and Y. Ding, *Nanoscale Adv.*, 2020, **2**, 3788–3797.
38 J. Zhang, A. Qiao, H. Tao and Y. Yue, *J. Non-Cryst. Solids*, 2019, **525**, 119665.
39 M. El Ouardi, H. A. Ahsaine, M. Zbair, A. BaQais and M. Saadi, *Chemosphere*, 2022, 136483.
40 A. Elaouni, M. El Ouardi, M. Zbair, A. BaQais, M. Saadi and H. A. Ahsaine, *RSC Adv.*, 2022, **12**, 31801–31817.
41 M. Y. BináZulkifli, *Chem. Commun.*, 2022, **58**, 12297–12300.
42 Z. Shi, K. Weng and N. Li, *Molecules*, 2022, **28**, 22.
43 Z. Shi, D. M. Di Toro, H. E. Allen and A. A. Ponizovsky, *Environ. Sci. Technol.*, 2005, **39**, 4562–4568.
44 G. Cao, *Nanostructures & nanomaterials: synthesis, properties & applications*, Imperial College Press, 2004.
45 J. T. Smith, E. M. Eckhardt, N. B. Hansel, T. Rahmani Eliato, I. W. Martin and C. P. Andam, *Microbiol. Spectrum*, 2022, **10**, e00201–e00222.
46 P. Kotrba, L. Dolečková, V. c. de Lorenzo and T. Ruml, *Appl. Environ. Microbiol.*, 1999, **65**, 1092–1098.
47 M. Zaidan, A. Noor Rain, A. Badrul, A. Adlin, A. Norazah and I. Zakiah, *Trop. Biomed.*, 2005, **22**, 165–170.
48 P. Ngamsurach and P. Praipipat, *RSC Adv.*, 2022, **12**, 26435–26454.
49 S. Soltani, K. Akhbari and J. White, *Polyhedron*, 2020, **176**, 114301.
50 S. Soltani, K. Akhbari and J. White, *J. Mol. Struct.*, 2020, **1214**, 128233.
51 V. T. Nguyen, V. T. Vu, T. H. Nguyen, T. A. Nguyen, V. K. Tran and P. Nguyen-Tri, *J. Compos. Sci.*, 2019, **3**, 61.